Electronic Supplementary Material (ESI) for Nanoscale.

Supporting Information

Easy to assemble PDMS/CNTs/PANI flexible supercapacitor with high energy-to-power density

Raphael D. C. Balboni,[a] Guilherme K. Maron,[a] Mateus G. Masteghin,[b] Mehmet O. Tas,[b] Lucas S. Rodrigues,[a] Veridiana Gehrke,[a] José H. Alano,[c] Robson Andreazza,[a] Neftali L. V. Carreño[a] and S. Ravi P. Silva[*b]

Experimental

All detailed information about calculation of areal and gravimetric specific capacitances, energy and power densities are described in detail, according to the following equations:

For measurements in three-electrode configuration, the areal specific capacitances (C_{spa}) were calculated according to the equation (1).

$$Cspa = \frac{i\ X\ \Delta t}{A\ X\ \Delta v} \qquad (1)$$

Where $Cspa$ is the areal specific capacitance, I is the discharge current, Δt is the discharge time, A is the area of the electrode (0.49 cm^{-2}) and ΔV is the potential range. The gravimetric specific capacitances (C_{spg}) were calculated according to equation (2).

$$Cspg = \frac{i\ X\ \Delta t}{m\ X\ \Delta v} \qquad (2)$$

Where m is the mass of polyaniline electrodeposited on the electrode. The gravimetric performances of the electrodes were based on the mass of PANI, since the mass of carbon nanotubes were difficult to reliably measure. Thus, the PDMS and the CNTs poorly contribute to the electrochemical performance of the device.

For measurements performed in the flexible symmetric two-electrode supercapacitors, the C_{spa} and C_{spg} were calculated from GCD curves according to the equation (3) and equation (4), using the area of both electrodes (total of 0.98 cm^2) and the mass of PANI of both electrodes, respectively.

$$Cspa = \frac{2I\int Vdt}{\Delta V^2 A} \qquad (3)$$

Where I is the current of charge/discharge, ∫Vdt is the area of the discharge curve after the IR drop, ΔV is the voltage window and A is the active area of the electrodes (0.98cm^2)

$$Cspa = \frac{4I\int Vdt}{\Delta V^2 m} \tag{4}$$

The areal and gravimetric energy densities were calculated from the GCD curves at different current densities, according to the equation (3)

$$Et = \frac{Csp \times \Delta v^2}{2 \times 3.6} \tag{5}$$

Where Et is the energy density, C_{sp} is the areal (or gravimetric) specific capacitance and ΔV is the potential range. The power density was calculated according to the equation (4)

$$Pt = \frac{Et}{\Delta t} \times 3600 \tag{6}$$

Where Pt is the power density, Et is the energy density and Δt is the discharge time.

For the cyclic voltammetry tests, the values of areal specific capacitances were obtained from the equation (5)

$$Cspa = \int 2\ idv/v\ \Delta E\ A \tag{7}$$

Where idv is the area of the curve, v is the scan rate, ΔE is the potential range and A is the area of a single electrode.

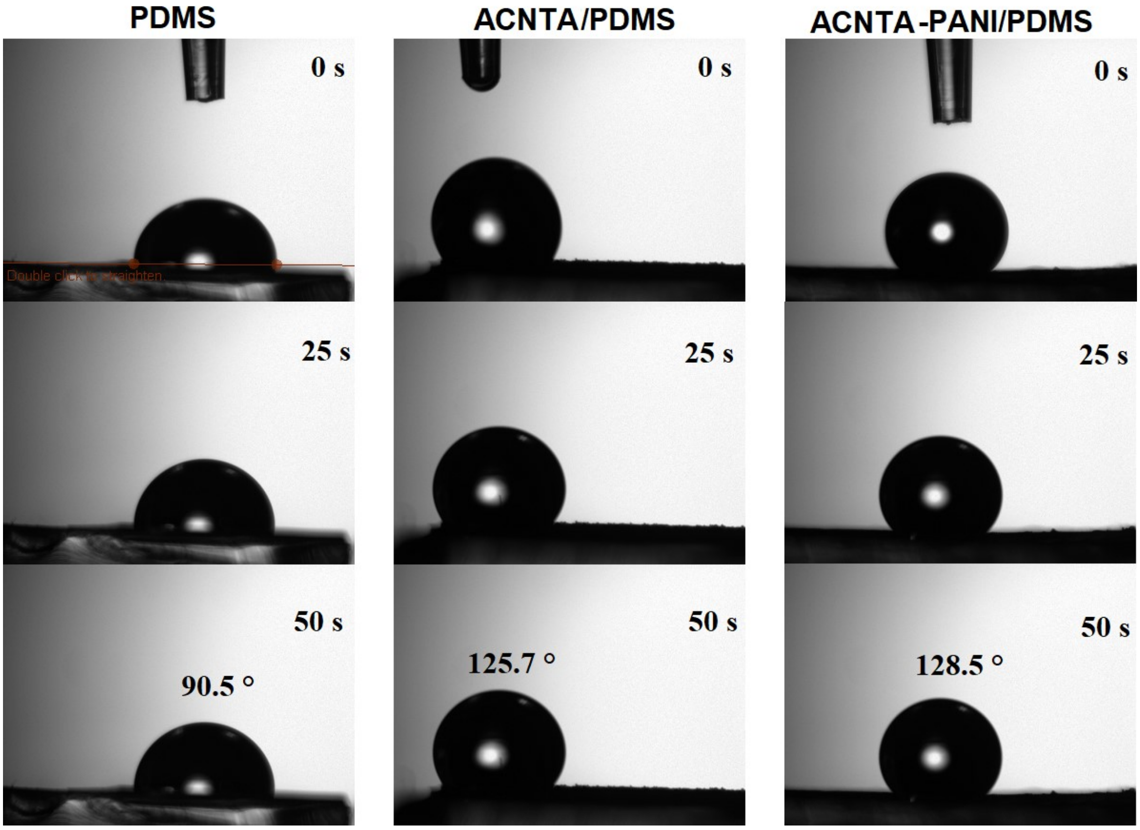

Fig. S1 Contact angle measurements of PDMS, ACNTA/PDMS and ACNTA-PANI/PDMS

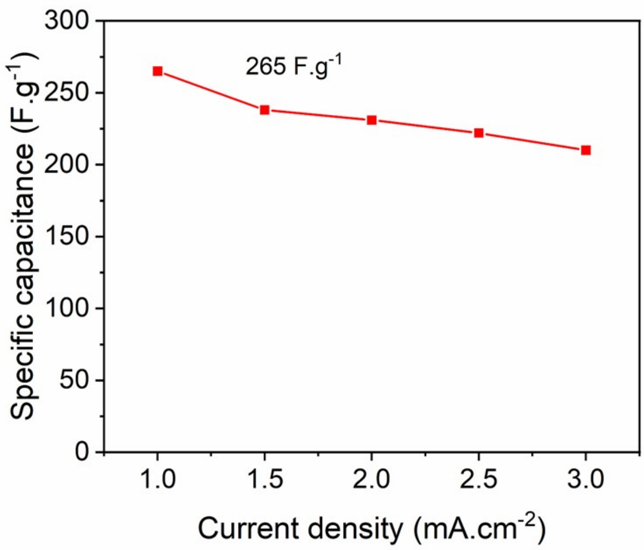

Fig. S2 Gravimetric specific capacitance calculated from GCD curves for the ACNTA-PANI/PDMS measured in three-electrode configuration

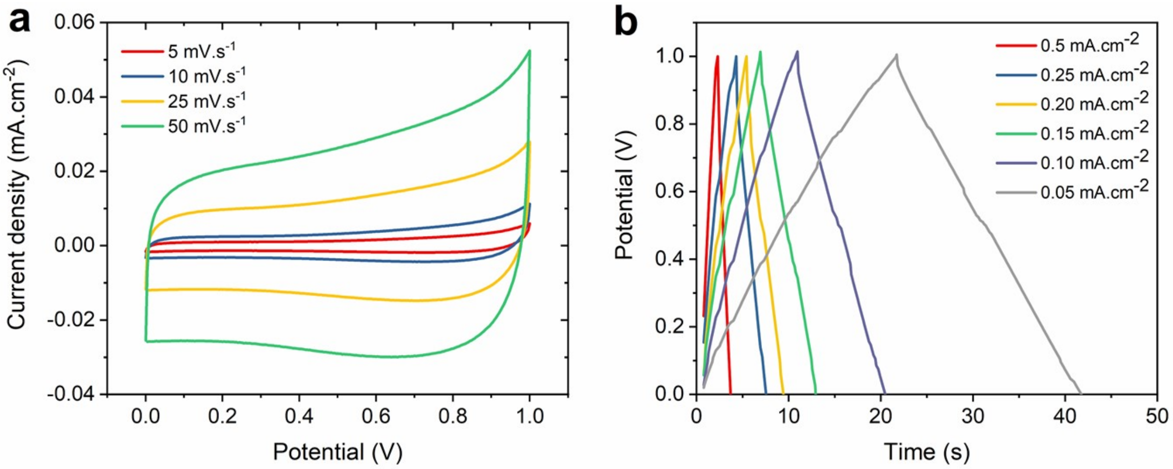

Fig. S3 Electrochemical performance of symmetric two-electrode ACNTA/PDMS supercapacitor. (a) CV curves at scan rates varying between 5 – 50 mV.s^{-1}. (b) GCD curves at different current densities

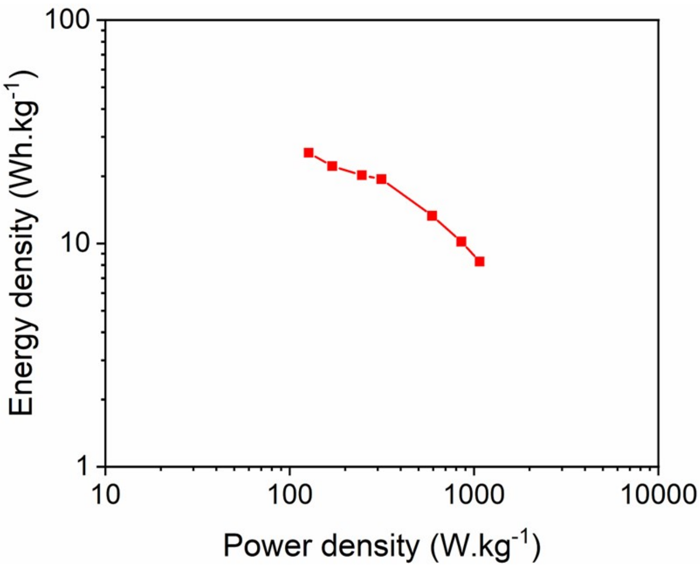

Fig. S4 Ragone plot showing the gravimetric energy and power densities calculated based on the mass of PANI

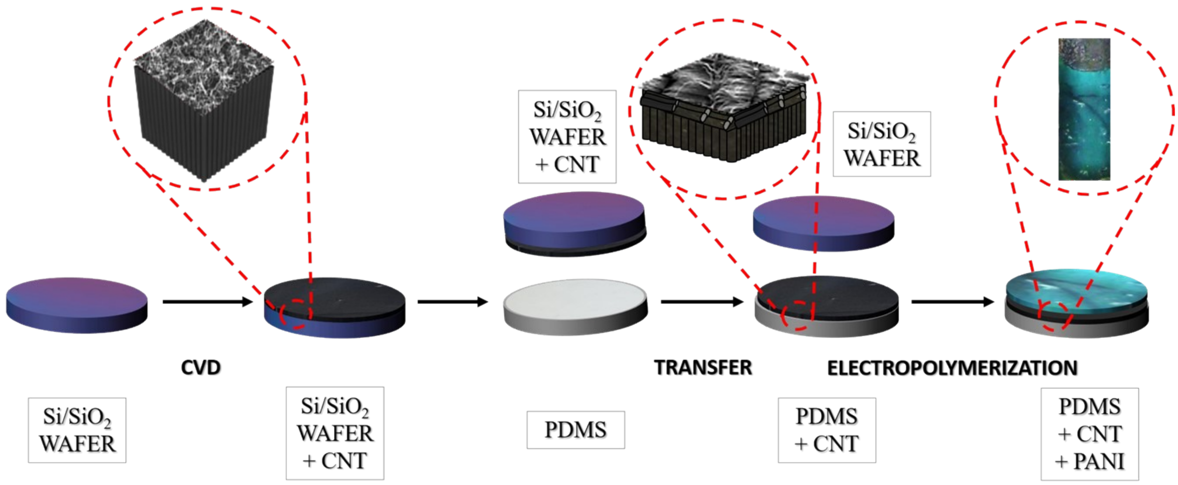

Fig. S5 Illustration of the electrode's fabrication process showing the steps between the initial Si/SiO$_2$ wafer and the final supercapacitor electrode. The vertically aligned carbon nanotubes (VA-CNTs) are grown at the activated metal catalyst on the surface of the buried oxide, which later is drop-casted facing a mild-cured PDMS, concluding the transfer process. The PDMS+CNT electrode then undergoes a PANI electropolymerization finalizing the fabrication of the flexible SC device

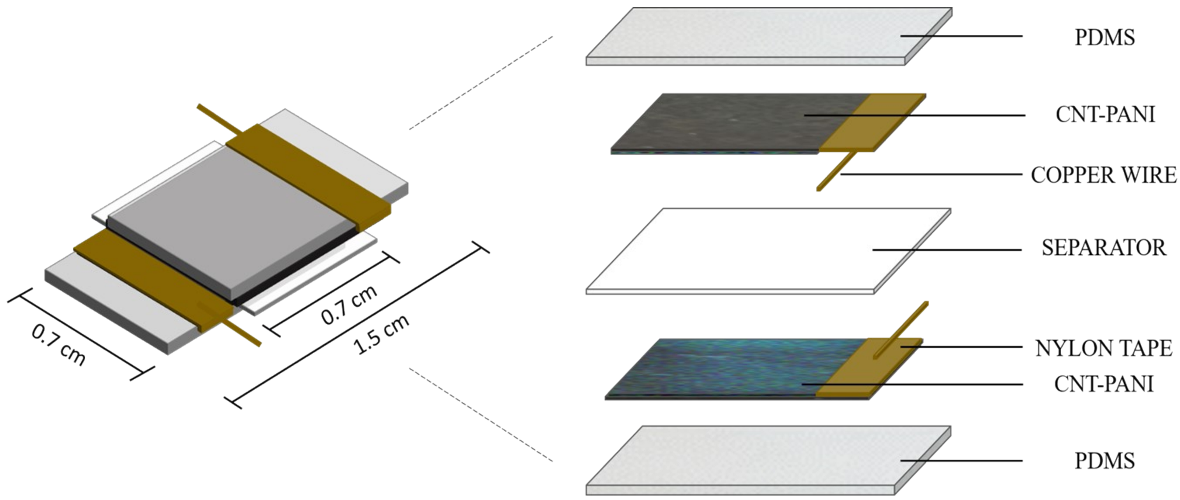

Fig. S6 Illustration of the flexible two-electrode supercapacitor assembly

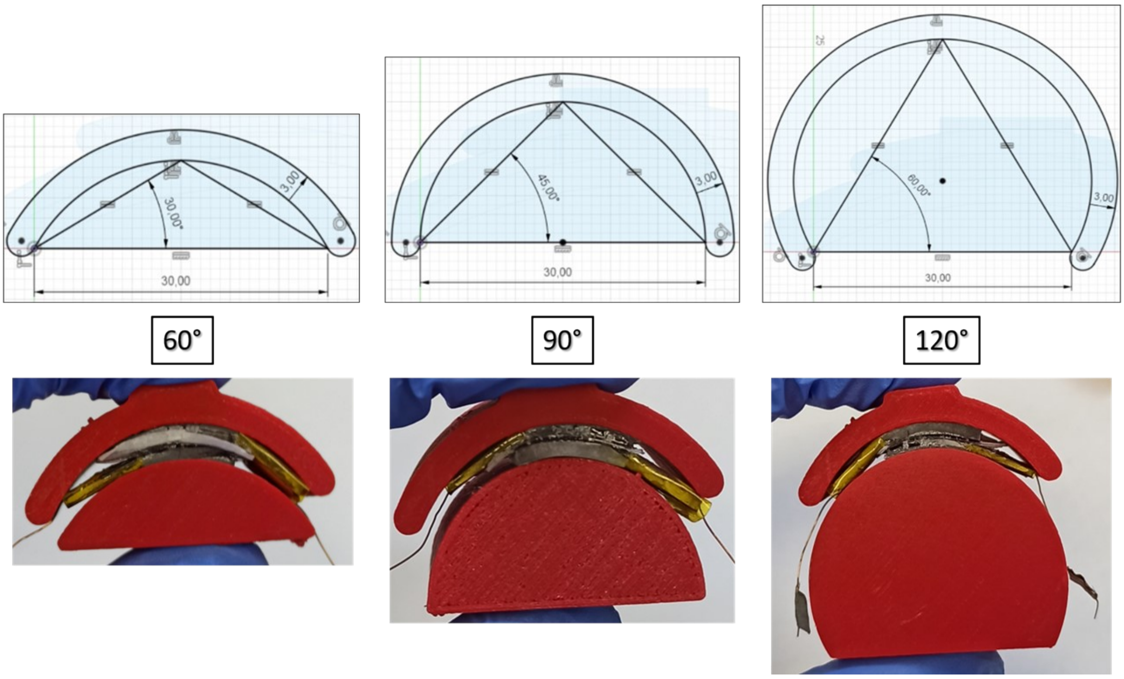

Fig. S7 Scheme illustrating the electrochemical measurements under different bending angles

Table S1 Comparison of areal and gravimetric specific capacitances of this work measured in two and three-electrode configurations with various similar materials for flexible supercapacitor application.

Sample	Measurement configuration	Current density	Scan rate	Csp ($mF.cm^{-2}$)	Csp ($F.g^{-1}$)	Ref
ACNTA-PANI/PDMS	Three-electrode	1 $mA.cm^{-2}$	-	408	265	**This work**
ACNTA-PANI/PDMS	Two- electrode	0.2 $mA.cm^{-2}$	-	40.6	51.6	**This work**
Ti3C2Tx/CF	Three-electrode	-	10 $mV.s^{-1}$		401	1
RuO2/CF	Three-electrode	-	10 $mV.s^{-1}$	-	388	1
a-MWCNT/PANI	Three-electrode	0.25 $A.g^{-1}$	-	-	201	2
PANI/VACNTs	Three-electrode	5 $A.g^{-1}$	-	-	415	3
PANI/MWCNT/PDMS	Three-electrode	-	5 $mV.s^{-1}$	481	-	4
Activated CC	Three-electrode	-	10 $mV.s^{-1}$	88	-	5
CNT@graphene@PANI/PDMS	Three-electrode	0.4 mA	-	588.7	-	6
VACNT-SS – TiO2	Two-electrode	1.67 $mA.cm^{-2}$	-	16.24	-	7
PPy(DBS)/CNTs/PDMS	Two-electrode	-	100 $mV.s^{-1}$	3.6	-	8
graphene/MoS2	Two-electrode	0.3 mA	-	70	-	9
MWCNT/PANI	Two-electrode	1 $A.g^{-1}$	-	-	233	10
CNT/MoS2/PDMS	Two-electrode	0.1 $mA.cm^{-2}$	-	-	10.67	11
PANI/MWCNT/PDMS	Two-electrode	-	5 $mV.s^{-1}$	-	159	4
MWCNTs-PANI-PDMS	Two-electrode	0.2 $mA.cm^{-2}$	-	44.13		12
CNT – PANI - PDMS	Two-electrode	1 $A.g^{-1}$			308.4	13
SWCNT-PDMS	Two-electrode	1 $A.g^{-1}$	-	-	54	12
3D-G/PANI/pdms	Two-electrode	1 $A.g^{-1}$	-	-	140	14
G-PANI	Two-electrode	0.1 $mA.cm^{-2}$	-	23	-	15
NRG//PANI	Two-electrode	0.25 $mA.cm^{-2}$	-	14.5	-	16
MOF/PANI	Two-electrode	0.1 $mA.cm^{-2}$	-	28.1	-	17

Table S2 Parameters obtained from the equivalent electric circuit from EIS measurements.

Sample	Rs ($ohm.cm^{-2}$)	C1 ($mF.cm^{-2}$)	R1 ($ohm.cm^{-2}$)	W	C2 ($mF.cm^{-2}$)
ACNTA/PDMS	214	6.99	209.7	7.2	1.04
ACNTA-PANI/PDMS	153.3	8.34	72.46	5.5	20.23

References

1 Q. Jiang, N. Kurra, M. Alhabeb, Y. Gogotsi and H. N. Alshareef, *Adv. Energy Mater.*, 2018, **8**, 1–10.

2 S. Y. Lee, J. Il Kim and S. J. Park, *Energy*, 2014, **78**, 298–303.

3 S. Hussain, E. Kovacevic, R. Amade, J. Berndt, C. Pattyn, A. Dias, C. Boulmer-Leborgne, M. R. Ammar and E. Bertran-Serra, *Electrochim. Acta*, 2018, **268**, 218–225.

4 M. Yu, Y. Zhang, Y. Zeng, M. S. Balogun, K. Mai, Z. Zhang, X. Lu and Y. Tong, *Adv. Mater.*, 2014, **26**, 4724–4729.

5 G. Wang, H. Wang, X. Lu, Y. Ling, M. Yu, T. Zhai, Y. Tong and Y. Li, *Adv. Mater.*, 2014, **26**, 2676–2682.

6 X. Liang, L. Zhao, Q. Wang, Y. Ma and D. Zhang, *Nanoscale*, 2018, **10**, 22329–22334.

7 P. Avasthi, A. Kumar and V. Balakrishnan, *ACS Appl. Nano Mater.*, 2019, **2**, 1484–1495.

8 R. Zhang, K. Yan, A. Palumbo, J. Xu, S. Fu and E.-H. Yang, *Nanotechnology*, 2019, **30**, 95401.

9 N. Li, T. Lv, Y. Yao, H. Li, K. Liu and T. Chen, *J. Mater. Chem. A*, 2017, **5**, 3267–3273.

10 H. Lin, L. Li, J. Ren, Z. Cai, L. Qiu, Z. Yang and H. Peng, *Sci. Rep.*, 2013, **3**, 1–6.

11 T. Lv, Y. Yao, N. Li and T. Chen, *Angew. Chemie - Int. Ed.*, 2016, **55**, 9191–9195.

12 L. Li, Z. Lou, W. Han, D. Chen, K. Jiang and G. Shen, *Adv. Mater. Technol.*, , DOI:10.1002/admt.201600282.

13 X. Chen, H. Lin, P. Chen, G. Guan, J. Deng and H. Peng, *Adv. Mater.*, 2014, **26**, 4444–4449.

14 K. Li, Y. Huang, J. Liu, M. Sarfraz, P. O. Agboola, I. Shakir and Y. Xu, *J. Mater. Chem. A*, 2018, **6**, 1802–1808.

15 X. Zang, X. Li, M. Zhu, X. Li, Z. Zhen, Y. He, K. Wang, J. Wei, F. Kang and H. Zhu, *Nanoscale*, 2015, **7**, 7318–7322.

16 L. Zhang, X. Qing, Z. Chen, J. Wang, G. Yang, Y. Qian, D. Liu, C. Chen, L. Wang and W. Lei, *ACS Appl. Energy Mater.*, 2020, **3**, 6845–6852.

17 A. P. M. Udayan, O. Sadak and S. Gunasekaran, *ACS Appl. Energy Mater.*, 2020, **3**, 12368–12377.